AIAA JOURNAL
Vol. 39, No. 11, November 2001

Aeroacoustic Characterization, Noise Reduction, and Dimensional Scaling Effects of High Subsonic Jets

J. C. Simonich* and S. Narayanan†
United Technologies Research Center, East Hartford, Connecticut 06108
T. J. Barber‡
University of Connecticut, Storrs, Connecticut 06269-3139
and
M. Nishimura§
Mitsubishi Heavy Industries, Ltd., Takasago, Hyogo 676-8686, Japan

A comprehensive far-field acoustics database was generated for high subsonic, turbulent jets along with mean total pressure and temperature surveys in the flowfield. The effects of core jet temperature and of external coflow on the far-field noise and mean flowfield characteristics are investigated. The results show peak jet noise generation in aft angles ($110 < \theta < 150$ deg). The mean velocity measurements indicate an average potential core length in the range of 3–8 jet diameters D_j, depending on the core jet flow temperatures and speed of external tunnel coflow, after which self-similar velocity decay is evidenced. Mixing devices (tabs) were used to enhance near-field jet mixing and were explored as a means for far-field noise reduction. These devices decreased the peak jet noise but were accompanied by increases in high-frequency noise. The effect of scaling from model-scale to engine-scale conditions shifts spectral peaks to lower frequencies, thereby driving high-frequency mixing noise increases (due to tab-generated flows) into the peak annoyance range.

Nomenclature

A	=	area
b	=	jet half-width
D	=	diameter of nozzle
H	=	shear layer shape factor
K	=	Witze proportionality constant, $0.08\,(1 - 0.16M_j)\,(\rho_e/\rho_j)^{-0.22}$
M	=	Mach number
P	=	pressure
Re	=	Reynolds number
r	=	radius
T	=	temperature
U	=	axial velocity component
x	=	axial coordinate, along jet axis
θ	=	observer angle, referenced to upstream
ρ	=	density
χ	=	x/r_j

Subscripts

a	=	ambient
cl	=	centerline
e	=	exit condition
f	=	full scale
j	=	jet condition
m	=	model scale
s	=	static condition
t	=	wind-tunnel condition, stagnation condition

Introduction

THE generation of noise from turbulent jets is of significant practicable interest, for example, for subsonic civil transport, and has received widespread attention for several decades. Noise has typically been measured and described by relatively simple characteristics such as level, frequency distribution, direction, and range. These characteristics have been reported to be a function of jet thrust, jet velocity, scale (dimension), jet composition (density, temperature, etc.), engine type, and supply or reservoir conditions. Historically, engine designers have achieved jet noise reduction through the decrease of engine exhaust velocities U_j, a feature derived from the U_j^8 scaling law contained in Lighthill's[1] benchmark theoretical research on aerodynamically generated sound. Lighthill's theory predicts that jet noise scales on the eighth power of jet speed, with a large range of experimental data corroborating this behavior. In Lighthill's first idealization of a jet, turbulence was regarded as the source of sound, a source characterized by the jet's speed and size. When such a model is followed, the mitigation of turbulence becomes a crucial step needed to reduce (aerodynamically generated) sound, and devising means to quiet turbulence becomes the challenge. Consequently, much of jet noise research has concentrated on understanding turbulence generation and associated noise, particularly in simple round jets, where complications arising due to complex flow phenomena and their interactions, for example, multiple shear layers, are avoided.

However, an understanding of the fundamental mechanisms underlying the generation of jet noise continues to remain a challenge. Computational techniques for aeroacoustics are still under development and remain limited in their use for reliable noise predictions in realistic flow conditions and geometries, for example, see the review by Tam.[2]

Because of the lack of understanding of the noise-generation process, experimental databases have represented the best source for developing analytical and computational models, for example, see Seiner[3] and Bridges and Podboy.[4] To date, however, there are few available databases having mean flow, turbulence, and far-field acoustics over relevant flight conditions, that is, heated, high-subsonic, high Reynolds number flows. The most noted of these limited databases have been published by Lush,[5] Lau,[6] Lau et al.,[7] Seiner and Norum,[8] and Lepicovsky.[9]

Seiner and Norum's[8] experiment was for a heated supersonic round jet without coflow. A water-cooled axisymmetric nozzle ($D = 3.6$ in.) (9.14 cm) was tested in the NASA Langley Research Center Jet Noise Laboratory. The nozzle design M_j was 2.0 at $T_{0j} = 2000$°F (1093°C). These conditions are much higher than of

Received 12 July 2000; revision received 10 April 2001; accepted for publication 18 April 2001.

*Senior Research Engineer, Acoustics. Senior Member AIAA.
†Research Engineer, Acoustics. Member AIAA.
‡Professor, Mechanical Engineering. Associate Fellow AIAA.
§Manager, Vibration and Control Laboratory.

interest to commercial engine applications. The nozzle operated at fully expanded conditions for the range of jet total temperatures considered in the test program. The flow Reynolds number, based on nozzle exit diameter D_j, varied from 2×10^6 to 3×10^6. Aerodynamic measurements of total temperature and total pressure were obtained and provided along the nozzle centerline using a water-cooled probe for a range of jet total temperatures. Additional data, that is, radial flow profiles and acoustic spectra, have not been provided. Over this range of temperatures, one can estimate the effects of compressibility in terms of the convective Mach number M_c. Whereas some far-field acoustics measurements were made, no turbulence data were reported.

An experimental program conducted at Lockheed by Lepicovsky[9] investigated mixing of near sonic heated round jets. A round nozzle having an exit diameter of 2.0 in. (5.08 cm) was examined over a range of jet total temperatures. No coflow was used in these experiments. Downstream total pressure and temperature axial and radial flow surveys were obtained using a United Sensor combined pressure and temperature probe. Boundary-layer surveys were obtained at the nozzle exit plane. These surveys confirm that, as the flow is heated to practical temperature levels, the Reynolds number decreases and eventually the flow transitions from turbulent ($H = 1.8$) at cold conditions to laminar ($H = 2.5$) at hot conditions. No turbulence or acoustic measurements were measured/published to complement the mean flow data.

Various passive control techniques have been proposed for jet noise reduction purposes. Flow control for mixing enhancement is relatively clear, that is, the goal is either to modify the large-scale turbulence structures in the flow or to generate new structures to enhance entrainment and mixing. Various nozzle geometry modifications such as lobed trailing edges, tabs, and simple in-plane cutouts along the trailing edges (also termed chevrons) have been used. Recently the role of streamwise vortex generators as effective mixers has been explored in detail. However, the details of the mechanisms of vortex generation, vortex interaction, and mixing scales in such devices are still sketchy. These devices have also been proposed and evaluated for noise reduction. An understanding of the noise reduction aspects of these devices is even poorer. The main reasons are as follows: 1) noise is a byproduct of turbulence, which in itself is not well understood; 2) measurement and understanding of noise is more involved than mixing because it involves not only the noise intensity but also frequency content and directionality; and 3) although intimately related, noise and flow are generally measured and studied separately due to the difficulties with facilities and instrumentation.

Passive devices, such as tabs (e.g., see studies by Zaman[10,11]) and flexible filaments,[12] and active devices, such as glow discharge[13] and pulsed-blowing-type actuators, have been considered, with mixed results. To date, only the passive tab and chevron approaches have demonstrated jet noise reduction in laboratory experiments (typically in supersonic jets).

The objective of the current study was generate a detailed benchmark aerodynamic and acoustic database for turbulent, high-speed, high Reynolds number, heated round jets and to evaluate flow control devices for jet noise reduction for full-scale turbofan engines.

Experimental Setup Description

The experiments were carried out in the United Technologies Research Center Acoustic Research Tunnel (ART) using a simple round nozzle (see Fig. 1). The tunnel is an open circuit design, which uses a 1500-hp (1.12-MW) fan to draw outside air through the open jet test section. A 36-in. (91.44-cm)-diam wind-tunnel nozzle was used for these tests. The test section is a $15 \times 18 \times 22$ ft ($4.57 \times 5.49 \times 6.71$ m) anechoic chamber, providing an anechoic environment down to 200 Hz. A jet mass flow rate of up to 10 lbm/s (4.54 kg/s) is achievable. A propane combustor supplies heated air up to 1000°F (538°C) for heated jet studies.

Mean velocity measurements were obtained using a three-probe rake consisting of a total pressure probe, a static pressure probe, and a total temperature probe. The three probes were mounted 2 in. (5.08 cm) apart on a double wedge wing support (diamond-shaped cross section) with a wedge half-angle of 7 deg. The pressure probes were close coupled to pressure transducers in the anechoic chamber to minimize the lags. The total pressure probe was a square edged, round pitot tube with a 0.0625-in. (1.588-mm) diam. The static pressure probe is similar to the one described by Pinckney.[14] Seiner and Norum[8] employed this same probe design in an earlier supersonic jet noise study. The total temperature probe was a double radiation shielded design with 0.25- and 0.12-in. (6.35- and 3.05-mm)-diam tubes.

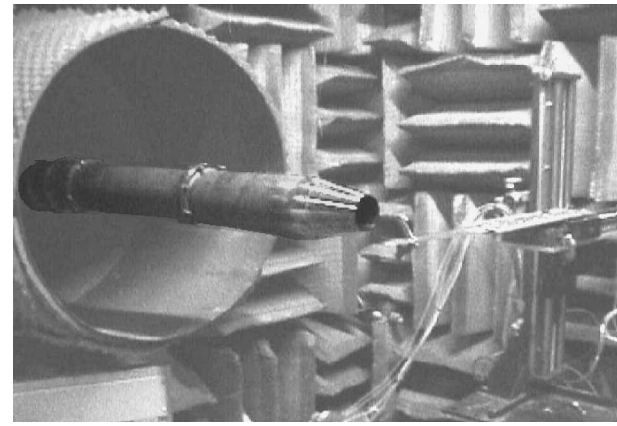

Fig. 1 Round nozzle installation and supersonic probe assembly in ART.

Data were obtained for both cold and hot turbulent jets (1000°F) (538°C) at high subsonic speeds ($M_j = 0.6$ and 0.9) and Reynolds number ($Re_D = 1.7 \times 10^6$). The nozzle diameter was 3.239 in. (8.23 cm) and is shown installed in the ART in Fig. 1. The model scale was approximately $\frac{1}{20}$th of a large, commercial full-scale jet engine [such as the V2500 with a fan tip diameter of 63.5 in. (1.61 m)]. The effect of forward flight on jet development was also examined with tunnel speeds up to $M_t = 0.3$. A variety of noise reduction techniques were investigated including flexible filaments[12] and small tabs[10,11] that are reported here.

Acoustic data were measured with a far-field array of eight B&K 4135 $\frac{1}{4}$-in. microphones at grazing incidence with the microphone grids removed. The array was located about 29.5 nozzle diameters from the nozzle centerline positioned at 10-deg increments from 80 to 150 deg relative to the upstream jet centerline axis to determine noise source directivity. The microphones were mounted 12 in. in front of 2×4 in. (5.08×10.16 cm) steel tube support beams that were covered with acoustic foam. Third octave and narrowband (250-Hz bandwidth) data were acquired sequentially using a bank of four Hewlett–Packard HP3451 spectrum analyzers. Pistonphone calibrations were performed for each data set acquired. The narrowband and one-third octave band sound pressure levels (SPL), from 50 Hz to 80 kHz, are stored together with relative humidity, temperature, and Mach number data. Adjustments to the processed data are made to subtract ART background noise and correct for atmospheric absorption.

The raw acoustic spectra were first corrected for high-frequency microphone response by applying individual microphone frequency calibration corrections to the data. The data were then converted to an ideal, loss-less day, that is, no attenuation due to humidity. Scaling to full scale was done by shifting the frequencies down by the ratio of the scale-to-full size diameters and increasing the amplitude by the full-scale to model-scale area ratio, namely, $10 \log_{10}(A_f/A_m)$. The data are then extrapolated to a standard 150-ft (45.7-m) radius. A weather correction is applied to the data to bring them to standard conditions [77°F (25°C) and 70% relative humidity]. Finally, noise metrics such as overall SPL (OASPL) and integrated perceived noise level (PNLI) are calculated from the data. For the single-stream jet studied here, the scaling to full scale is more applicable to low bypass ratio engines with mixed streams than to high bypass ratio engines with separate streams.

The acoustic results from jet noise reduction concepts at model scale were converted to be representative of the full-scale engine size, and perceived noise levels were predicted to evaluate their potential for jet engine application. Scaling of measured model data

to full scale and extrapolating to 150-ft (45.7-m) radial distance is then needed for comparison to full-scale or engine conditions.

The scaling to full-scale engine[15] is accomplished by shifting the model scale spectra "to the left" (in frequency space) by a model-to-engine scale factor. For example, the 80-kHz one-third octave frequency band of model jet noise spectra becomes the 4-kHz one-third octave band for an engine 20 times larger. Because the resulting full-scale spectra have missing values, for example, 6.3 kHz, 8 kHz, etc., these values are filled in using an assumed jet noise high-frequency rolloff rate of 3 dB per one-third octave band. The extrapolation to 150-ft (45.7-m) radius is accomplished by using corrections for spherical divergence and atmospheric absorption for the additional extrapolated distance.

In addition to far-field acoustics measurements reported here, a phased microphone array was also utilized to determine the noise source location. A detailed description of the phased array system is provided elsewhere.[16] A companion paper[17] describes the results of hot-wire and source distribution measurements for the same jet conditions and discusses the effect of turbulence on jet noise generation.

Noise Metrics

The sound emitted from a general sound source varies in frequency content with directivity. Basic laboratory noise measurements are made without weighting the sound over a frequency spectrum. One measure of the total energy being emitted by a noise source at a given directivity angle is the OASPL. This is determined by integrating the noise over the spectrum. However, for the same amplitude level, the human ear perceives some frequencies louder than others.

There are several metrics that have been developed to better relate the human perception of noise at different frequencies. An example is the A-weighted SPL used by many commercial sound level meters. For aircraft noise, a perceived noise level (PNL) was developed for this purpose. The PNL is a subjective assessment of the perceived noisiness of aircraft noise. The PNL levels are calculated by correcting measured third octave levels using a standard noy table. A noy is a subjectively developed measure of equivalent noisiness.

The noise certification of aircraft is governed in the United States by Federal Aviation Regulation (FAR) 36 (Ref. 18) and internationally by International Civil Aviation Organization flyover noise regulations.[19] The noise level of a single aircraft operation is described by an effective PNL (EPNL). It is derived from the instantaneous PNL by applying corrections for pure tones and for the duration of the noise. The formulas used to compute the EPNL are given in FAR 36 Appendix B.[18]

Database Results

Jet Physics

The jet external flowfield is typically divided into three characteristic regions: 1) a potential core region in which mixing is initiated in the shear layers from the nozzle lip, leaving a region of uniform, essentially inviscid, velocity close to the jet exit velocity: 2) a far-field decay or similarity region, where the mixing rate is nominally proportional to the inverse of the axial distance from the nozzle, $1/x$ [radial profiles of flow properties can be superimposed under an appropriate scaling, e.g., $U/U_j \approx f(y/b_{1/2})$], where $b_{1/2}$ is the radial location where the velocity is half the core velocity; and 3) a transition region from region 1 to region 2. These characteristics can be extracted from either experimental or computational data by identifying the end of the potential core ***Xc*** and the slope of the far-field decay rate ***n***, obtained from the scalar variables (velocity, Mach number, temperature), that is,

$$U/U_{\mathrm{cl}} = (x/D)^{-n}$$

$$\log(U/U_{\mathrm{cl}}) = -n\log(x/D)$$

This expression can be obtained from similarity arguments for turbulent round jets. Empirical evidence, obtained by Witze,[20] indicates that the centerline data for heated jets over a range of exit Mach number conditions follows a more elaborate form, that is, for large x,

$$U/U_{\mathrm{cl}} = 1-\exp\{\alpha/[1-(x/x_c)]\} \Rightarrow 1-\{1+[\alpha/1-(x/x_c)+\cdots]\}$$

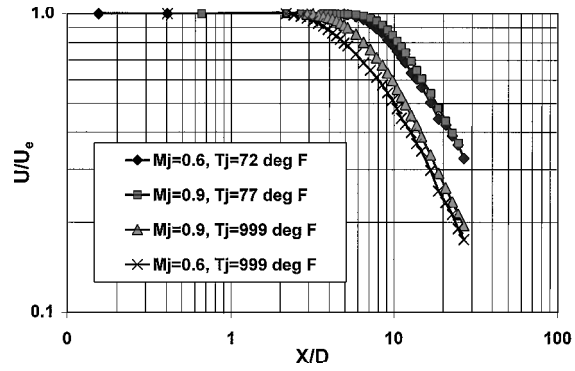

Fig. 2 Centerline velocity decay for cold and heated round jets; $M_j = 0.6$ and 0.9.

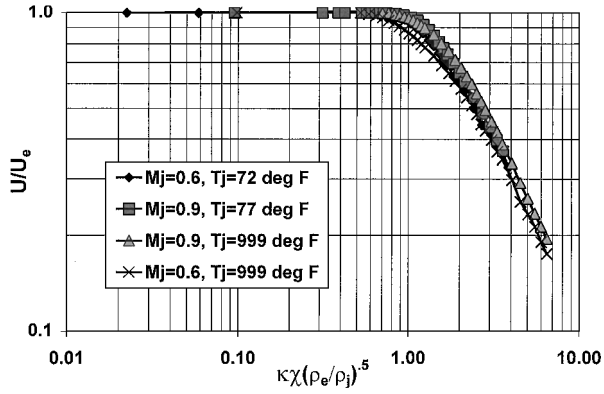

Fig. 3 Centerline velocity decay plotted using Witze[20] axial correlation parameter.

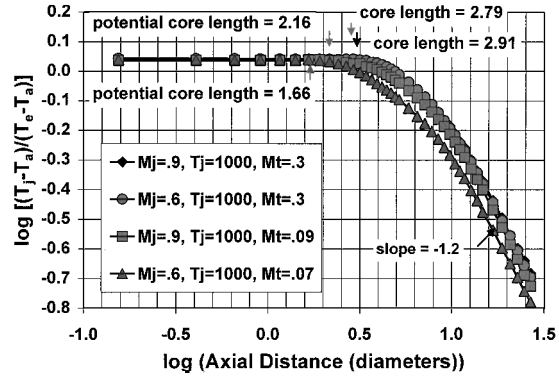

Fig. 4 Effect of jet Mach number and coflow on the jet temperature decay rate.

and therefore

$$\log(U/U_{\mathrm{cl}}) = \log\{\alpha/[1-(x/x_c)]\} \Rightarrow \log[\alpha x_c/x]$$

where α is a constant. Therefore, for large x/x_c, the two scaling laws agree when the far-field decay rate n is -1.

Aerodynamic Results

Measurements of the jet centerline velocity and temperature were made as a function of the streamwise distance for several jet Mach numbers, temperatures, and coflow velocities. The velocity decay along the jet centerline as a function of jet Mach number and jet exit temperature is shown in Fig. 2. The length of the potential core is seen to increase with Mach number while decreasing with temperature. These same data are shown in Fig. 3 using the Witze[20] axial correlation parameter $\kappa\chi(\rho_e/\rho_j)^{0.5}$. The use of the parameter appears to collapse the four different operating points. A similar result for the centerline temperature decay is shown in Fig. 4. Clearly, the ambient tunnel flow impacts the jet mixing characteristics.

From these data, displays in a log–log format were generated, and the length of the potential core and rate of mixing were determined.

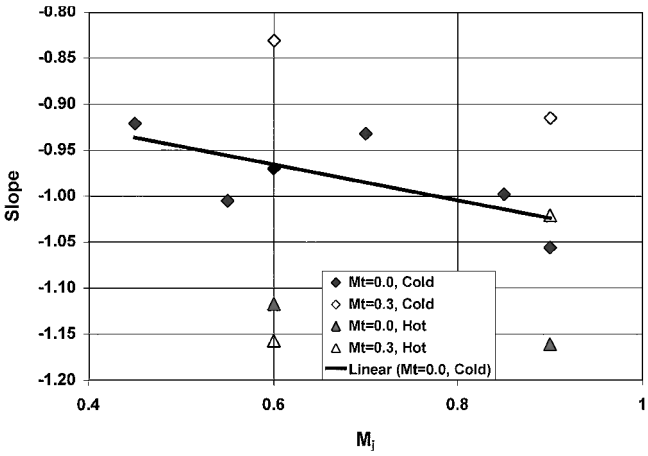

Fig. 5 Slope of centerline velocity far-field decay rate.

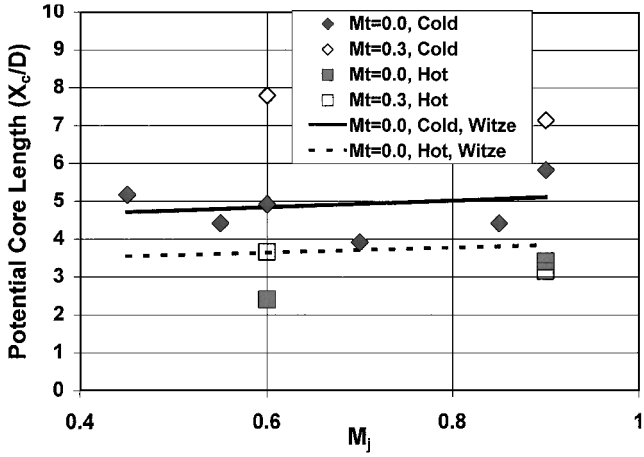

Fig. 6 Length of velocity potential core for round jet.

Figure 5 shows the slope of the log–log jet centerline velocity vs distance curve as a function of jet Mach number, temperature, and tunnel speed. It is seen that coflow increases the length of the velocity core. Care has been taken to obtain sufficient data in the transition region from the potential core region to the far-field decay region (where the largest noise is believed to be generated). Figure 6 shows the potential core length as a function of jet Mach number for cold and heated jets, with and without coflow. The potential core lengths predicted by Witze[20] for static jet conditions (no coflow) are also shown. Use of the Witze scaling predicts a small increase in core length with jet exit Mach number and a substantial decrease in core length with heating. Both trends are consistent with current results.

When considering heated jets, one needs to consider the velocity rather than the Mach number, thereby isolating thermal effects on mixing. Mean flow aerodynamics data were obtained for jet exit Mach numbers ranging from 0.45 to 0.90, with and without coflow, as well as for cold and heated jets. Results demonstrate the effect of jet exit flow, coflow, and heating on the potential core length and on the far-field decay of temperature and velocity.

The decay results are referenced to the classical $(x/D)^{-n}$ expression, where n is the far-field decay rate. The velocity slope for a cold static jet matches the previously published results of Lau[6] and Lau et al.[7] These results clearly confirm previous[21,22] observations for heated jets that the temperature slope is greater than the velocity slope, that is, the rate of thermal mixing is greater than momentum mixing. Other observations are that heating increases the rate of momentum mixing, whereas coflow decreases it; heating decreases the length of the velocity core, whereas coflow increases the core length; and heating and coflow influence the thermal mixing rate or thermal potential core.

Radial profiles of total pressure, static pressure, and total temperature were recorded using the probes described earlier. These results were processed to produce a local Mach number using two separate

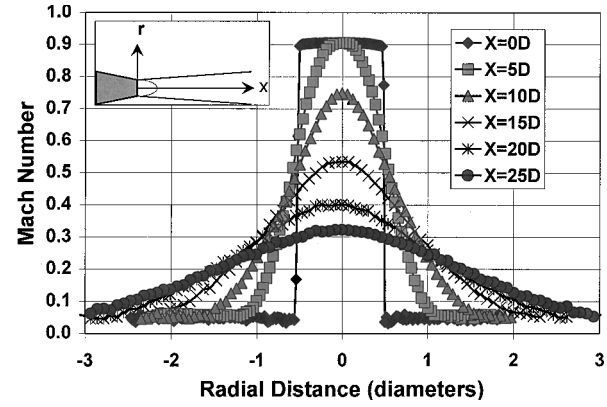

Fig. 7 Radial Mach number profiles for $M_j = 0.9$, cold, no coflow, using chamber static pressure.

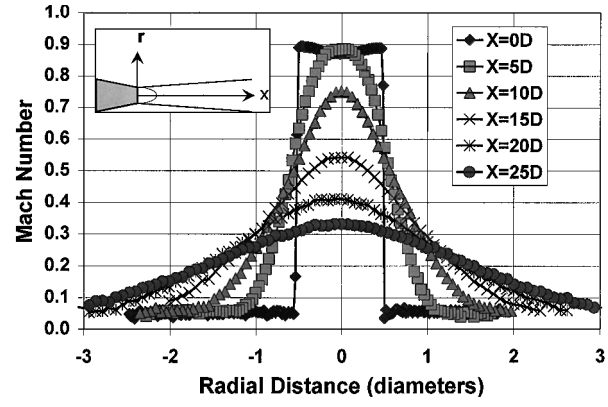

Fig. 8 Radial Mach number profiles for $M_j = 0.9$, cold, no coflow, using local static pressure.

approaches: 1) using local P_T and the chamber static pressure (note that most jet measurements do not measure the local static pressure) and 2) using the local P_T and P_S values. These results are shown for a static (without coflow) $M_j = 0.9$ cold jet in Figs. 7 and 8. In the case where the Mach number is derived from the chamber static pressure, the velocity has a flat-top profile. However, the Mach number derived from the local P_S initially exceeds the jet exit value. If one looks closely at the $x/D_j = 0$ profiles in Figs. 7 and 8, it can be seen that P_S is not close to ambient in the jet near field.

Acoustic Results

A representative set of baseline jet acoustic data is shown in Fig. 9. The test condition was $M_j = 0.9$ [$T_j = 1000$°F (538°C)], with no forward flight effect ($M_t = 0.0$). These data are shown to be in good agreement with the semi-empirical code data of Ref. 23. The shape of the noise spectra changes with observation angle from a symmetric, round hump shape at angles perpendicular to the jet to a non-symmetric pattern at angles approaching the downstream jet axis. The frequency of the peak noise decreases from around 3 kHz at angles perpendicular to the jet to around 1 kHz at angles close to the jet axis. The peak amplitude of the measured jet spectra increases in downstream angles, in good agreement with the predicted trend in Ref. 23.

There are some undulations in the low frequencies of the third octave data whose source is yet unclear. The anechoic quality of the chamber was checked by extensive acoustic decay measurements, and no problems were observed above 200 Hz. The "lumpiness" of the spectra may have been caused by standing waves set up by reflections from the microphone support beams. The steel beams were covered with acoustic foam that is known to be ineffective at low frequencies. The support-induced reflections and potential contamination of acoustic spectra at low frequencies has since been verified.

A study was also conducted to examine the repeatability of baseline third octave data for $M_j = 0.6$ and 0.9, hot and cold conditions.

As expected, the repeatability of the cold data was better than the hot data. The maximum differences between two runs for the four cases are given in Table 1.

A comparison between measured narrowband results and the empirically derived spectral shape from Tam et al.[24] for the $M_j = 0.9$, $T_j = 1000°$F (538°C) jet is shown in Fig. 10. The "Tam fine-scale spectral model" is shown at 80 deg, whereas the "Tam large-scale spectral model" is shown at 140 deg. The peak amplitude and its frequency for the empirical fit were shifted to best fit the measured data. The spectral shapes agree quite well except at very high frequencies.

Flow and Noise Control Results

Experiments were performed for the round nozzle with small tabs[10,11] mounted at the trailing edge of the nozzle (Fig. 11). The tabs are triangular in cross section, angled into the flow at 45 deg, and have a trailing edge angle of 90 deg, consistent with recommendations in Refs. 10 and 11. The tab configurations tested consisted of 0.25-in.-wide, 0.19-in.-long, 0.012-in.-thick, stainless steel triangles. Configurations studied included two, four, six, and eight tabs, equally distributed around the jet exit plane.

Figure 12 shows acoustic spectra at $M_j = 0.9$ for the eight-tab configuration, in cold conditions, in conventional coordinates (SPL vs frequency) along with equivalent baseline round jet spectra. A jet noise reduction at peak frequencies is evident, but a high-frequency increase is also noted. The actual level of the high-frequency noise is at a significantly lower decibel level. A more realistic view of these acoustic results is to consider their effect in a full-scale (nominally chosen at 20 times larger) implementation.

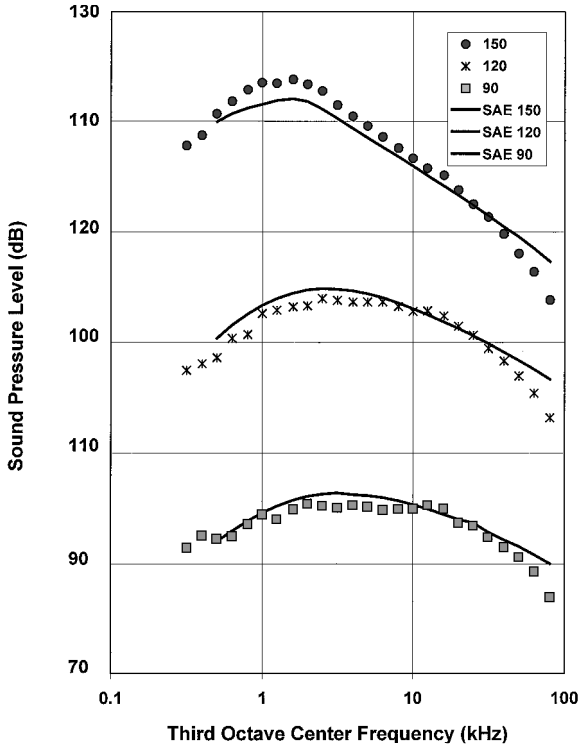

Fig. 9 Third octave spectra for $M_j = 0.9$, $T_j = 1000°$F (538°C), baseline and predictions[23] (ordinate scale offset for ease of viewing).

Three spectra for the 130-deg orientation (Figs. 13–15) are compared to the baseline round nozzle. The measured spectra in model scale are shown in Fig. 13. The effect of scaling (Fig. 14) is to shift the model scale spectra to the left by a factor of 20. The scaling approach is cited by Soderman,[15] where one assumes that acoustic spectra remain unchanged when scaled by a nondimensional frequency, the Strouhal number. With this assumption, when a constant velocity jet U_j is scaled up in size D, the resultant spectra f shifts proportionately to the left. The effect of human annoyance (noy weighting) is then applied (Fig. 15). One can clearly see that the low-frequency noise reduction is more than offset by the high-frequency mixing noise, which is now located in the peak annoyance range.

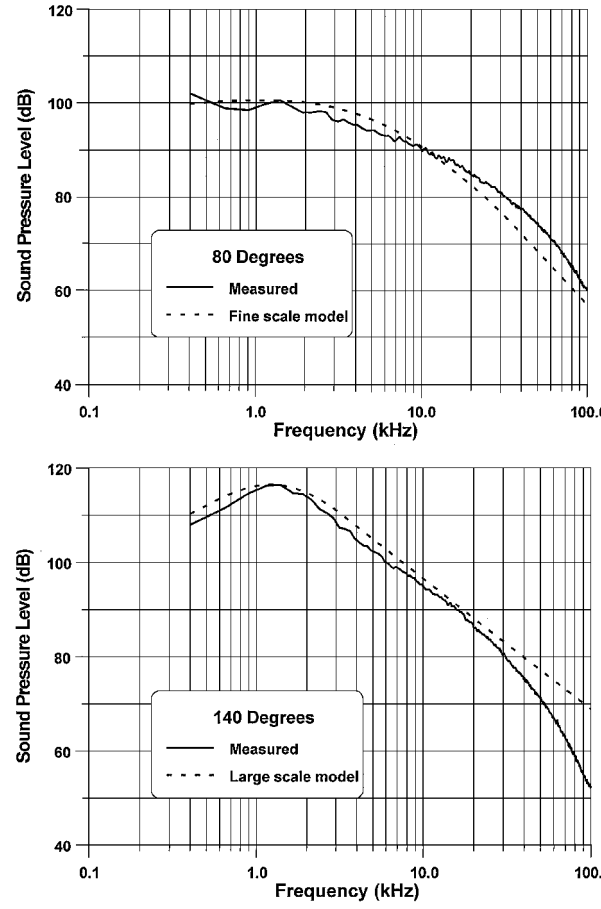

Fig. 10 Comparison of measured narrowband spectra at $M_j = 0.9$, $T_j = 1000°$F (538°C) with Tam et al.[24] model.

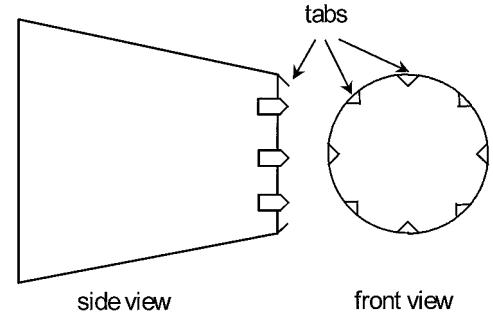

Fig. 11 Small tabs at the trailing edge of a round nozzle.

Table 1 Experimental repeatability

	Third octave dB		Velocity, ft/s (m/s)		Temperature, °F (°C)	
Mach number	Maximum−minimum	Standard deviation	Maximum−minimum	Standard deviation	Maximum−minimum	Standard deviation
0.6, cold	0.50	0.26	9 (2.7)	1.5 (0.46)	——	——
0.9, cold	0.80	0.33	6 (1.8)	0.2 (0.061)	——	——
0.6, $T_j = 1000°$F (538°C)	1.40	0.42	26 (7.9)	6.4 (1.9)	20 (11)	4.8 (2.7)
0.9, $T_j = 1000°$F (538°C)	1.80	0.51	18 (5.5)	6.2 (1.9)	11 (6)	2.2 (1.2)

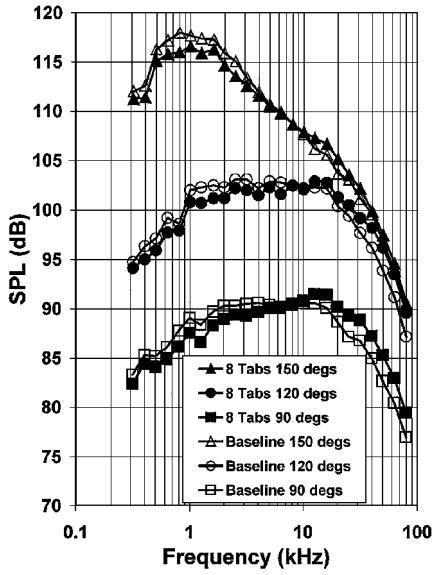

Fig. 12 Third octave spectra for $M_j = 0.9$, cold, baseline and eight-tab jets.

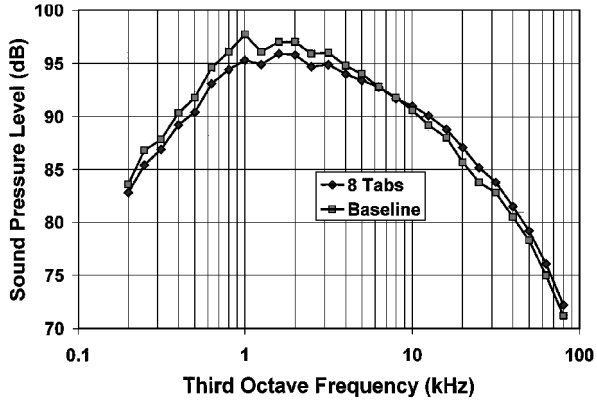

Fig. 13 Model-scale spectrum for eight-tab case, $M_j = 0.6$, $T_j = 1000°$F (538°C), 130 deg.

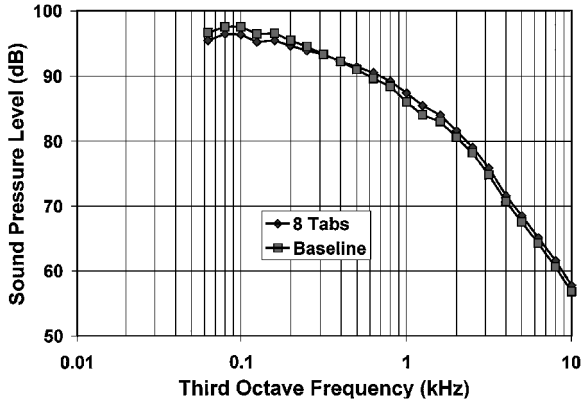

Fig. 14 Full-scale spectra (20 X), eight tabs, $M_j = 0.6$, $T_j = 1000°$F (538°C), 130 deg.

A contour plot (Fig. 16) is presented, which summarizes the results for the cold six- and eight-tab acoustic results. A complete acoustic data set is represented in each plot. The data are plotted as the difference in SPL in decibels between the tab mounted on the round nozzle trailing edge and the baseline round nozzle. The darker gray contour areas are indicative of noise reduction with tabs. The lighter gray contours represent noise increases over the baseline.

The $M_j = 0.6$ and 0.9 results are similar, showing some noise reduction. The two-tab and four-tab data showed a slight increase in noise at high frequencies. The largest effect occurred for the six-

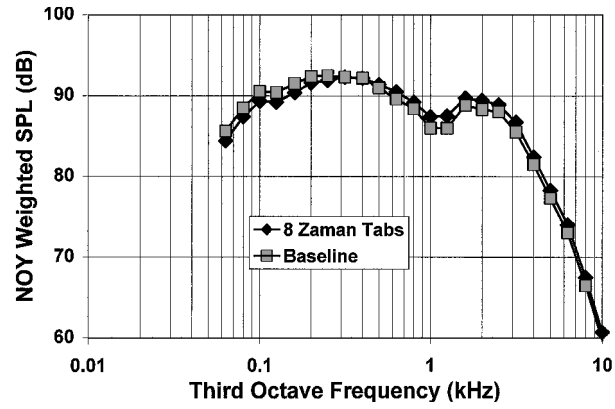

Fig. 15 Noy weighted spectrum for eight-tab case, $M_j = 0.6$, $T_j = 1000°$F (538°C), 130 deg.

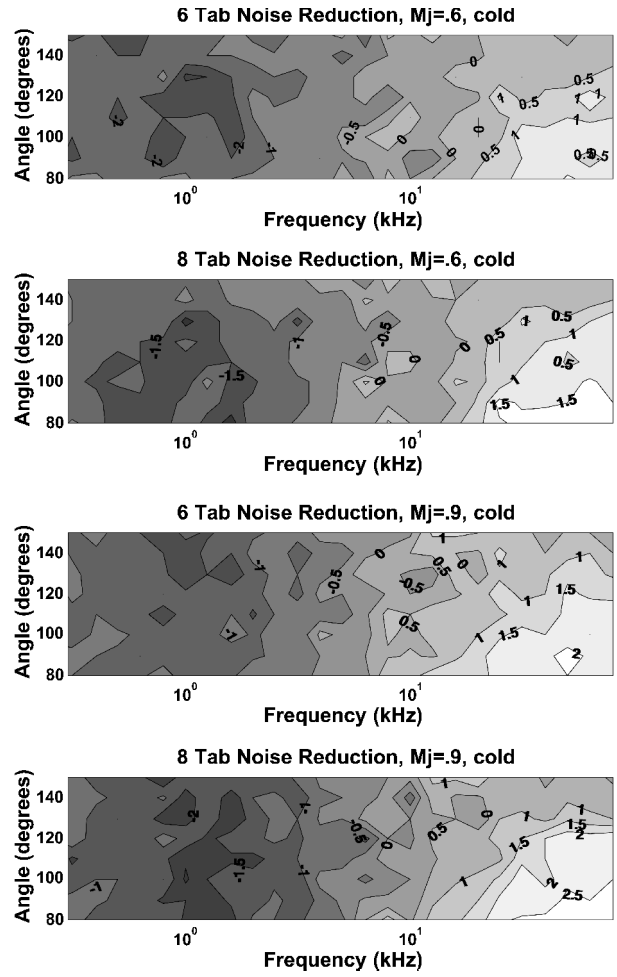

Fig. 16 Spectral shift of tab nozzles from baseline, cold jets.

and eight-tab cases. At low to mid frequencies near the jet noise peak (300 Hz–3 kHz), 1–2 dB of noise reduction was achieved. However, there is a large increase in high-frequency noise, particularly at sideward angles. The highest increase is seen in the bottom right corner of the eight-tab, $M_j = 0.9$ plot at the bottom of Fig. 16. The best tab configuration appears to be the six-tab case because it had nearly the same noise reduction at midfrequencies as the eight-tab case, but with less increase in high-frequency noise. There was also a large noise increase at high frequencies noted for the four-tab case at $M_j = 0.9$, which is not as apparent for $M_j = 0.6$.

The acoustic performance of the tab configurations and conditions tested was evaluated via a PNLI. The PNLI is the log sum of the PNL at all microphone angles. These results are summarized in Table 2. All cases show an increase in PNLI over the baseline round nozzle

Table 2 Tab PNLs compared to baseline

Number of Zaman[10,11] tabs	M_j	T_j, °F	Δ PNLI, dB
2	0.6	59	0.21
2	0.9	57	0.55
4	0.6	58	0.30
4	0.9	58	0.57
6	0.6	54	0.16
6	0.9	52	0.65
8	0.6	57	0.33
8	0.9	58	0.88
2	0.6	1000	0.32
2	0.9	1000	0.39
4	0.6	1000	0.17
4	0.9	1000	0.90
6	0.6	1000	0.27
6	0.9	1000	0.66
8	0.6	1000	0.27
8	0.9	1000	0.48

Table 3 Flexible wire PNLs compared to baseline round jet

String length diameter	Number of strands	Length after knot diameter	M_j	ΔPNLI, db
3	2	——	0.6	0.02
3	2	——	0.9	0.40
3	2	0	0.6	0.34
3	2	0	0.9	0.32
5	2	——	0.6	−0.08
5	2	——	0.9	0.08
2	——	1	0.6	0.13
2	——	1	0.9	−0.03
4	6	——	0.6	0.21
4	6	0.2	0.6	0.34
5	6	0.3	0.6	1.14
5	6	0.3	0.9	1.38
3	——	0.3	0.9	1.90
3	9	——	0.9	0.26
2	9	——	0.9	0.24
4	Many	——	0.6	1.18
4	Many	——	0.9	0.28
3	Many	——	0.9	0.04
3	Many	——	0.6	0.79
3	Many	——	0.6	0.21

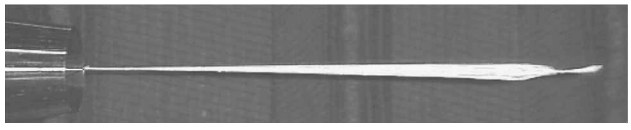

Fig. 17 Flexible wire operating in $M_j = 0.6$ cold jet.

from 0.16 to 0.9 PNLI dB. This indicates that although model-scale peak noise reduction was achieved, these devices are unlikely to be beneficial in full-scale engines.

Flexible Filaments

The use of a flexible string[12] for jet noise reduction was tested at $M_j = 0.6$ and 0.9 for $T_j =$ cold and 300°F (149°C). A flexible filament mounted in the center of a jet interacts with the flow in a yet undetermined manner to effect the jet noise. Its use is appealing for jet engines because it could be deployable and not suffer a drag penalty at cruise, which many passive devices incur. A multistranded, unbraided Kevlar® string was used for both cold and warm conditions. A photograph of the flexible filament(s) at the exit of the jet nozzle is shown in Fig. 17.

A robust material has not yet been found for high-temperature operation. The string was attached to 0.010-in. (0.254-mm)-diam cross support wires in the center of the nozzle exit with a small knot. Support wires of this size were shown not to effect the baseline acoustics. The length of the string was varied from 2 to 5 jet diameters. The thickness was approximately 0.02 jet diameters. A knot was typically placed at the end of the string.

The noise reductions observed were similar to those obtained by Anderson et al.[12] Noise reductions achieved were also similar to those obtained with the small tabs. Noise reductions of 1–2 dB were observed in the low to midfrequency range, but increases of 1–2 dB were seen in the high-frequency region. The PNLI results are shown in Table 3. Except for a couple of cases, possibly due to measurement error, all cases displayed increased PNLI.

Summary

A benchmark database for round, heated, high-speed jet acoustics and aerodynamics is presented, which can be used to validate (perhaps tune) noise prediction models. The passive noise reduction concepts tested in model scale, using a flexible string and small tabs, were shown to reduce peak jet noise amplitude by 1–2 dB. However an increase in high-frequency jet noise was observed for both devices. The six-tab configuration appears to be optimum because it has the maximum peak noise reduction with the smallest high-frequency noise increase (penalty). However, full-scale estimates, with frequency shifting and noy weighting for the model-scale data, nullify the peak jet amplitude reduction and intensify the high-frequency noise effect, resulting in an overall perceived noise level increase. Extreme caution must be exercised when using model-scale results to predict full-scale trends.

Acknowledgments

We appreciate the financial support provided for this program by Pratt and Whitney (East Hartford) and Mitsubishi Heavy Industries. The authors would like to thank R. W. Paterson, R. H. Schlinker (United Technologies Research Center), W. Lord, D. Mathews, F. Stern, V. Saxena, and L. Bock (Pratt and Whitney) for insightful discussions. The authors are grateful to T. Kudo (Mitsubishi Heavy Industries, Ltd.) for his assistance in data reduction and processing for the aerodynamics and acoustics data.

References

[1]Lighthill, M. J., "On Sound Generated Aerodynamically: I. General Theory," *Proceeding of the Royal Society*, Vol. 211A, No. 1101, 1952, pp. 564–587.

[2]Tam, C. K. W., "Jet Noise: Since 1952," *Theoretical and Computational Fluid Dynamics*, Vol. 10, No. 1, 1998, pp. 393–405.

[3]Seiner, J. M., "A New Rational Approach to Jet Noise Reduction," *Theoretical and Computational Fluid Dynamics*, Vol. 10, 1998, p. 373.

[4]Bridges, J., and Podboy, G. G., "Measurements of Two-Point Velocity Correlations in a Round Jet with Application to Jet Noise," AIAA Paper 99-1966, May 1999.

[5]Lush, P. A., "Measurements of Subsonic Jet Noise and Comparison with Theory," *Journal of Fluid Mechanics*, Vol. 46, No. 3, 1971, pp. 477–500.

[6]Lau, J. C., "Effects of Exit Mach Number and Temperature on Mean-Flow and Turbulence Characteristics in Round Jets," *Journal of Fluid Mechanics*, Vol. 105, 1981, pp. 193–218.

[7]Lau, J. C., Morris, P. J., and Fisher, M. J., "Measurements in Subsonic and Supersonic Free Jets Using a Laser Velocimeter," *Journal of Fluid Mechanics*, Vol. 93, 1979, pp. 1–27.

[8]Seiner, J. M., and Norum, T. D., "Experiments of Shock Associated Noise on Supersonic Jets," AIAA Paper 79-1526, 1979.

[9]Lepicovsky, J., "An Experimental Investigation of Nozzle-Exit Boundary Layers of Highly Heated Free Jets," American Society of Mechanical Engineers, ASME Paper 90-GT-255, June 1990.

[10]Zaman, K. B. M. Q., "Effects of Delta Tabs on Mixing and Axis Switching in Jets from Axisymmetric Nozzles," AIAA Paper 94-0186, Jan. 1994.

[11]Zaman, K. B. M. Q., "Spreading Characteristics of Compressible Jets From Nozzles of Various Geometries," *Journal of Fluid Mechanics*, Vol. 383, 1999, pp. 197–228.

[12]Anderson, B., Wygnanski, I., and Gutmark, E., "Noise Reduction by Interaction of Flexible Filaments With an Underexpanded Supersonic Jet," AIAA Paper 99-0080, Jan. 1999.

[13]Corke, T. C., and Cavalieri, D. A., "Controlled Experiments on Instabilities and Transition to Turbulence in Supersonic Boundary Layers," AIAA Paper 97-1817, June 1997.

[14]Pinckney, S. Z., "A Short Static-Pressure Probe Design for Supersonic Flow," NASA TN D-7978, July 1975.

[15]Soderman, P. T., "On the Scaling of Small-Scale Jet Noise to Large Scale," *Proceedings of the DGLR/AIAA 14th Aeroacoustics Conference*, Deutsche Gesellschaft für Luft- und Raumfahrt e.V. (DGLR), Bonn, 1992, p. 663.

[16]Saligrama, V., Polak, D., and Narayanan, S., "Phased Array Design, Validation, and Application to Jet Noise Source Localization," AIAA Paper 2000-1934, June 2000.

[17]Narayanan, S., Barber, T., and Polak, D., "High Subsonic Jet Experiments, Part II: Turbulence and Noise Generation Studies," AIAA Paper 2000-2023, June 2000.

[18]"Noise Standards: Aircraft Type and Airworthiness Certification," Federal Aviation Administration, FAR Pt. 36, June 1974 (consolidated reprint 12 Aug. 1985).

[19]*Annex 16–Environmental Protection*, Vol. 1, *Aircraft Noise*, 3rd ed., International Civil Aviation Organization, Montreal, QC, Canada, 1993.

[20]Witze, P. O., "Centerline Velocity Decay of Compressible Free Jets," *AIAA Journal*, Vol. 12, No. 4, 1974, pp. 417, 418.

[21]Landis, F., and Shapiro, A. H., "The Turbulent Mixing of Co-Axial Gas Jets," Heat Transfer and Fluid Mechanics Inst., Stanford Univ. Press, Stanford CA, 1951.

[22]Schetz, J. A., *Injection and Mixing in Turbulent Flow*, Vol. 68, Progress in Astronautics and Aeronautics, AIAA, New York, 1980, pp. 35–38.

[23]"Gas Turbine Jet Exhaust Noise Prediction," Society of Automotive Engineers, SAE Rept. ARP876, issued 1978-03, rev. 1994-01.

[24]Tam, C. K. W., Golebiowski, M., and Seiner, J. M., "On the Two Componenets of Turbulent Mixing Noise from Supersonic Jets," AIAA Paper 96-1716, May 1996.

P. J. Morris
Associate Editor